Calibration-less sizing and quantitation of polymeric nanoparticles and viruses with quartz nanopipettes

Péter Terejánszky, [±,‡] István Makra,[±,‡] Péter Fürjes,[§] Róbert E. Gyurcsányi[±]*

[±]MTA-BME "Lendület" Chemical Nanosensors Research Group, Department of Inorganic and Analytical Chemistry, Budapest University of Technology and Economics, Szt. Gellért tér 4, Budapest, 1111 Hungary

[§] MEMS Laboratory, HAS Research Centre for Natural Sciences, Konkoly-Thege út 29-33, Budapest, 1121 Hungary

*corresponding author: robertgy@mail.bme.hu (Fax: +36-1-463 3408)

KEYWORDS Quartz nanopipette, counting and sizing nanoparticles, resistive pulse sensing, poliovirus

Author Contributions

The manuscript was written through contributions of all authors. All authors have given approval to the final version of the manuscript.

‡These authors contributed equally.

ABSTRACT The feasibility of using quartz nanopipettes as simple and cost-effective Coulter counters for calibration-less quantitation and sizing of nanoparticles by resistive pulsing sensing (RPS) was investigated. A refined theory was implemented to calculate the size distribution of nanoparticles based on the amplitude of resistive pulses caused by their translocation through nanopipettes of known geometry. The RPS provided diameters of monodisperse latex nanoparticles agreed within the experimental error with those measured by using scanning electron microscopy (SEM) and dynamic light scattering (DLS). The nanopipette-based counter, by detecting individual nanoparticles could resolve with similar resolution as SEM mixtures of monodisperse nanoparticles having partially overlapping size distributions, which could not be discriminated by DLS. Furthermore, by calculating the hydrodynamic resistance of the nanopipettes and consequently the volume flow through the tip enabled for the first time the calibration-less determination of nanoparticle concentrations with nanopipettes. The calibration-less methodology is applied to sizing and quantitation of inactivated poliovirus of ca. 26 nm diameter, which is the smallest size spherical shape virus ever measured by resistive pulse sensing.

GRAPHICAL ABSTRACT
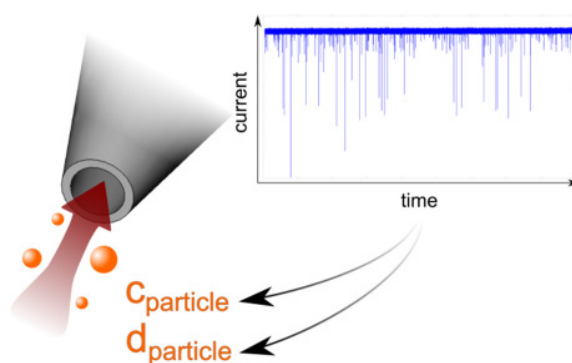
INTRODUCTION

Owing to the importance of determining the size distribution and concentration of nanoparticles of synthetic or natural origin in liquid media a variety of characterization methods have been developed. These methods include: (i) *separation techniques*, such as size exclusion chromatography,[1] flow field-flow fractionation,[2] electrophoretic techniques,[3] and analytical ultracentrifugation;[4] (ii) *light scattering methods* stemming size information from the particle's Brownian motion on the basis of Stokes-Einstein equation, e.g., dynamic light scattering (DLS) and nanoparticle tracking analysis (NTA)[5]; (iii) *imaging methods*, e.g., scanning probe and electron microscopy techniques. These methods, are generally used in a complementary fashion as none of them is able to offer, at least not routinely, simultaneous size, shape and concentration information without removing the nanoparticles from their natural liquid environment. Presently, DLS is the gold standard to assess the size distribution of nanoparticles in suspensions due to the rapid and non-invasive way in which nanoparticles can be characterized in an extremely broad size and solvent range. However, the severe limitations of DLS in terms of resolving polydisperse nanoparticle suspensions with close size distributions gives the way to sizing methodologies that are based on the direct detection of individual nanoparticles and therefore have superior size resolution. Thus, DLS measurements are commonly complemented with high resolution imaging of nanoparticles, most often by electron microscopy, to provide their size and shape. Such measurements are generally made with nanoparticle preparates on a solid surface that may not entirely reflect the properties of the nanoparticles in their natural liquid environment. Individual nanoparticle detection, however, is feasible also in solution phase with optical and electrochemical methods. Emerging techniques include NTA which provides both size and concentration information by tracking the motion of individual nanoparticles based on their light scattering,[6] as

well as resistive pulse sensing (RPS)[7] and amperometric electrode-nanoparticle collision-based electrochemical techniques[8]. In special, RPS by using single-nanopore counters offers unique advantages such as wide applicability in terms of detectable nanoparticles (in contrast to collision-based electrochemical methods[8, 9]), ease of miniaturization,[10] and the possibility of providing information on the shape,[11-13] deformability,[14] and surface charge[15, 16] of nanoparticles. RPS implies monitoring changes (pulses or peaks) in the voltage driven ion current across a nanopore that separates two electrolyte chambers as particles are passing through.[7] The frequency of the resistive pulses is a measure of the nanoparticle concentration while their amplitude and shape are indicative of the nanoparticle size and geometry. The size range of resistive pulse based counters is relatively narrow, i.e., for classical Coulter counters comprising pores with diameters in the μm range is ca. 2 to 60% of the pore diameter[7] compared to ca. 4 orders of magnitudes that can be assessed by DLS. Thus, while it is feasible to extend the detectable size range either by the ingenious approaches of using size-tunable elastomeric pores,[17] node-pore sensing[18] or simply by using pores of different diameters, the niche of nanopore-based counters seems to be the sensing of specific size nanoparticles by properly tuned pore sizes rather than of a universal nanoparticle characterization device. In this respect counting and characterizing the size distribution of virus particles contours as a major prospective application of RPS.[18-23] Viruses are generally characterized by a very narrow size distribution falling in a size range that provides a better prospective of distinguishing them from most constituents of biological fluids,[22] e.g., proteins and cells. Indeed, while the feasibility of detecting smaller species, e.g., nucleic acids[24, 25], proteins,[26] and even organic molecules[27] have been convincingly demonstrated in ideal conditions their applicability in practical situations without using specific receptors[28-30] may be rendered very difficult by the large variety of similarly sized species coexistent in real samples. Several attempts

have been already to characterize viruses starting from the proof of principle of their detectability by RPS,[19, 31] which include monitoring antibody-virus interactions in real time[20] as well as capsid characterization studies.[32] However, most of the RPS applications in general do not provide quantitative concentration and size information on the counted nanoparticles but stop at the stage of reporting rough current amplitude and frequency histograms as well as their relative changes.[20, 21, 32] In this study we were interested to assess the performance of RPS for quantitative sizing and counting of nanoparticles in the size range relevant to virus counting and to compare the results with DLS and SEM measurements. The methodology was worked out by using latex nanoparticles and was applied for quantifying and sizing poliovirus, which, to our best knowledge, with its size of 24-30 nm,[33-35] is the smallest spherical shaped virus ever measured by RPS.

From the plethora of nanopores and materials reported for RPS[36, 37], which includes biological protein pores,[38] silicon nitride,[39] polymers,[19, 40-42] glass,[43-45] quartz,[46] elastomers,[23] as well as carbon nanotubes[47, 48] we have chosen to use quartz nanopipettes.[49] Our choice was motivated by the fact that probably none of the nanopore technologies reported can compete with the availability, wide size range, cost-effectiveness, ease and extremely short preparation times of nanopipettes by pulling quartz capillaries. Still, studies on using nanopipettes for nanoparticle sizing are rather scarce[45, 46] and, their capabilities as nanoparticle counters for providing both quantitative size and concentration information have not yet been explored. In principle, as shown for other type of nanopores,[50, 51] knowing the geometry of the pipette tip, the amplitude of the resistive pulses caused by translocating spherical nanoparticles can be used to determine their diameter without the need of particle size standards.[23] Similarly, the nanopore geometry can be used to calculate the hydrodynamic resistance of the pore and consequently the volume flow rate in pressure driven counting experiments to provide calibration-less estimates of the particle

concentrations as shown for elastomeric nanopores.[17] As the greatest resistance change in conical nanopores is expected when only a part of the nanoparticle is in the nanopipette interior we have used the theoretical model developed by Willmott and Parry,[52] which accounts for the access resistance changes caused by the out-of pore section of the nanoparticle. Therefore, the present study is expected to provide more accurate size distributions as attempts[45] that consider only the resistive contribution of the nanoparticles within the nanopore.[27]

Experimental Section

Chemicals and materials

Spherical shape carboxylate-modified latex nanoparticles (CML) with 4% w/v concentration and nominal diameters of 110 nm (110 nm); 73 nm (69 nm); 67 nm (68 nm); 45 nm (55 nm) were purchased from Life Technologies Corporation (Carlsbad, CA). The values in parenthesis are diameters determined by SEM in this study. Inactivated and viability tested poliovirus samples (Sabin-1 strain) were provided by the National Center of Epidemiology (Hungary). Quartz capillaries of 1 mm outer and 0.7 mm inner diameter with filament, were obtained from Sutter Instrument Co. (Novato, CA).

Fabrication of nanopipette-based nanoparticle counters

Quartz nanopipettes were fabricated by pulling quartz capillaries with a microprocessor controlled micropipette puller (P-2000, Sutter Instrument). A two-cycle pulling program was used: Cycle 1 (Heat 750; Filament 4; Velocity 55; Delay 132; Pull 55) and Cycle 2 (Heat 800; Filament 3; Velocity 30; Delay 129; Pull 70) resulting in nanopipettes with ca. 800 nm diameter. For smaller diameter pipettes the pull value in Cycle 2 was increased while keeping all other parameters constant, e.g., for the smallest 50 nm diameter nanopipette a pull value of 200 was used. The

nanopipettes were filled with electrolyte and the electrical connection was established by inserting a Ag/AgCl wire attached to a polycarbonate holder comprising also a pressure port. For RPS measurements, custom made cells of either 0.1 or 1 mL volume were used comprising an electrolyte/sample solution and a Ag/AgCl wire reference/counter electrode (Fig. S1).

Electrochemical measurements

For electrical resistance and counting measurements a HEKA EPC 10 USB patch-clamp amplifier was used, with the electrodes connected through a low-noise headstage to the instrument. Both the cell and the headstage were placed in a Faraday cage. The resistance of the nanopipettes was calculated from current changes measured upon applying two consecutive 10 ms duration square wave pulses with ±10 mV amplitude in an electrolyte solution; for nanopipette size estimation in 1 M KCl solution containing 0.05% Triton-X100. Counting experiments were performed at constant voltage ($100 \leq E_{appl} \leq 300$ mV) the value of which depended on the noise level and translocation frequency. Two analog filters were used in series (5-pole and 4-pole Bessel filters) with an effective bandwidth of 7.3 or 10 kHz and a sampling rate of 200 kHz. Quantitation of the nanoparticles was performed by applying a negative pressure (typically, $0 \leq \Delta p \leq 1000$ Pa) adjusted with a manometer, to aspirate the sample suspension through the tip in the pipette interior. Fifty mM KCl with 0.05% Triton-X100 adjusted to pH 10 was used to count CML nanoparticles, while poliovirus counting was performed in PBS with 0.05% Tween-20 at pH 7.4. In all cases the same solution was used in the sample compartment and the pipette interior.

Nanoparticle characterization by DLS and SEM

DLS measurements were performed by using Zetasizer NanoZS (Malvern Instruments Ltd., UK) in backward scatter mode. For sizing particles by SEM a LEO 1540XB ultrahigh resolution field emission SEM system (Carl Zeiss AG, Oberkochen, Germany) was used. Nanoparticles suspended in DI water were drop casted onto the surface of a Si wafer, dried at room temperature and SEM images were acquired (see Supporting Information for details).

THEORY

The overall resistance of the nanopipette-based electrochemical cell is dominantly determined by the smallest constriction of the nanopipette, i.e., by the resistance of the tip. Therefore, the contribution of the cylindrical part of the pipette is not considered in this treatment. The shape of the tip can be approximated by a truncated cone and accordingly its resistance can be calculated by using a finite length conical geometry as shown in Fig. 1.
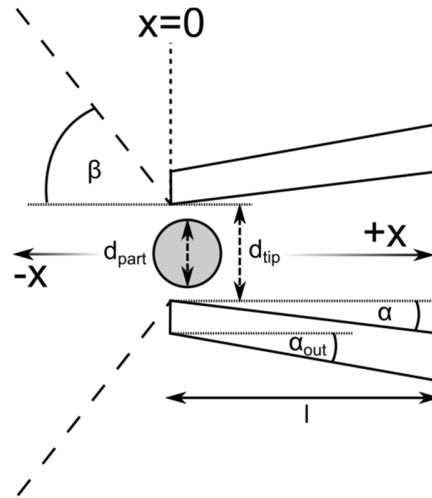
Figure 1. Schematic of the conical geometry nanopipette tip with a nanoparticle residing in its sensing zone

If the surface conduction effects are minimized by using high ionic strength solution the nanopipette resistance ($R_l^{pipette}$) is given by Eq. 1:

$$R_l^{pipette} = \frac{1}{\sigma} \int\limits_{x=0}^{l} \frac{1}{A(x)} dx = \frac{4l}{\pi d_{tip}\sigma(d_{tip} + 2\tan(\alpha)l)} \qquad \text{Eq. 1}$$

where σ is the bulk conductivity of the solution, $A(x)$ is the cross-section of the nanopipette, x is the coordinate along the pipette axis, d_{tip} is the diameter, α the inner half-cone angle and l the length of the pipette tip, respectively. Because the length of a nanopipette tip is at least 3 orders of magnitude longer than the tip diameter one can approximate Eq. 1, which is the most extensively used expression for the resistance of a conical pore,[27, 53] with its infinite length version:

$$\lim_{l\to\infty} R_l^{pipette} = R^{pipette} = \frac{2}{\pi d_{tip}\sigma \tan(\alpha)} \qquad \text{Eq. 2}$$

However, for a full treatment the resistive contribution of the out-of-pipette part of the sensing zone originating from the convergence of the electric field lines, i.e., the access resistance (R^{access}), should also be considered. For R^{access} we have used the expression derived by Hall.[54]

$$R = R^{pipette} + R^{access} = \frac{2}{\pi d_{tip}\sigma \tan(\alpha)} + \frac{1}{2d_{tip}\sigma} \qquad \text{Eq. 3}$$

Particle translocation model

In this study nanoparticles are treated as electrical insulators of spherical shape and the solution conductivity in the nanopore is considered constant and equal to that of the solution bulk. Therefore, nanoparticles passing though the sensing zone of the nanopipette, focused at the tip proximity, are causing transitory decreases in the transpore current (negative pulses or peaks). To calculate the amplitude of the current pulses we have used the model developed recently by Willmott and Parry,[52] which considers the out-of-tip access zone as a second truncated cone connecting to the nanopore entrance through its top circle and having a half-cone angle of $\beta = arctan\left(\frac{4}{\pi}\right) \approx 51.85°$ (Fig. 1). At this particular angle the infinitely long "access" cone will have the same resistance as the access resistance. With these assumptions, the resistance of a nanopipette

having a particle within its sensing zone (R_{part}) can be calculated using Eq. 1 for the two conical

sections, i.e., tip and out-of-tip access zone, with the alteration that $A(x)$ is now the cross section

not occupied by the particle. To calculate the resistance change during particle translocation, the

particle is placed at different positions along the x axis and the resistances are calculated as

described above (see Supporting information for analytical solutions). Of note, this model might

slightly underestimate the relative current changes as it assumes parallel electric field lines around

the nanoparticles, which especially for very small particles is not true.[19] Fig. 2 A and B show the

calculated relative current changes as a function of the particle position along the x coordinate for

different relative particle sizes ($\frac{d_{part}}{d_{tip}}$) and nanopipette half cone angles, respectively. The relative

current change is roughly proportional to the nanoparticle-to-pore (sensing zone) volume ratio,

and accordingly are relatively small, e.g., less than 4 % for particles close to the upper detectable

size limit ($\frac{d_{part}}{d_{tip}} = 0.6$) for a nanopipette with $\alpha = 8°$, a representative value for nanopipettes used

in this study. As the volume of the sensing zone is strongly dependent on the half cone angle of

the tip the relative current change increases by using tips with larger angles. However, the half

cone angle also impacts the sensing zone length, l_{sens}, defined here as the length where the signal

is higher than 5% of its maximum value. The sensing length consists of two sections, a shorter one

($l_{sens,out}$) in the access cone outside the pipette and a longer ($l_{sens,in}$), which is inside the pipette.

Larger cone angles increase the contribution of $l_{sens,out}$ to the total sensing length, e.g., for a

relative particle size of 0.5 from less than 2 % at 1° to ca. 12 % at 10° and a similar trend is observed

if the relative particle size increases (Figs. S2, S3). Of note, while using tips with larger α is

beneficial in terms of increasing the amplitude of the current pulses, it also leads to shorter sensing

zones and consequently smaller pulse durations requiring larger bandwidths to minimize pulse distortion.
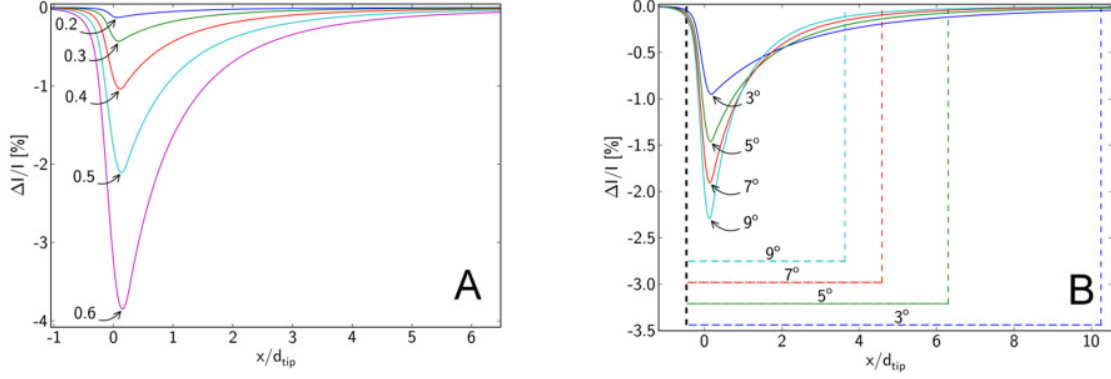
Figure 2. Relative current changes as a function of the particle position along the pipette axis for (A) a nanopipette with $\alpha = 8^{\circ}$ at different d_{part}/d_{tip} ratios and (B) for nanopipettes with different α at $d_{part}/d_{tip} = 0.5$. The length of the sensing zone is indicated by dashed lines for each half-cone angle. At *x*=0 the center of the particle is at the tip orifice.

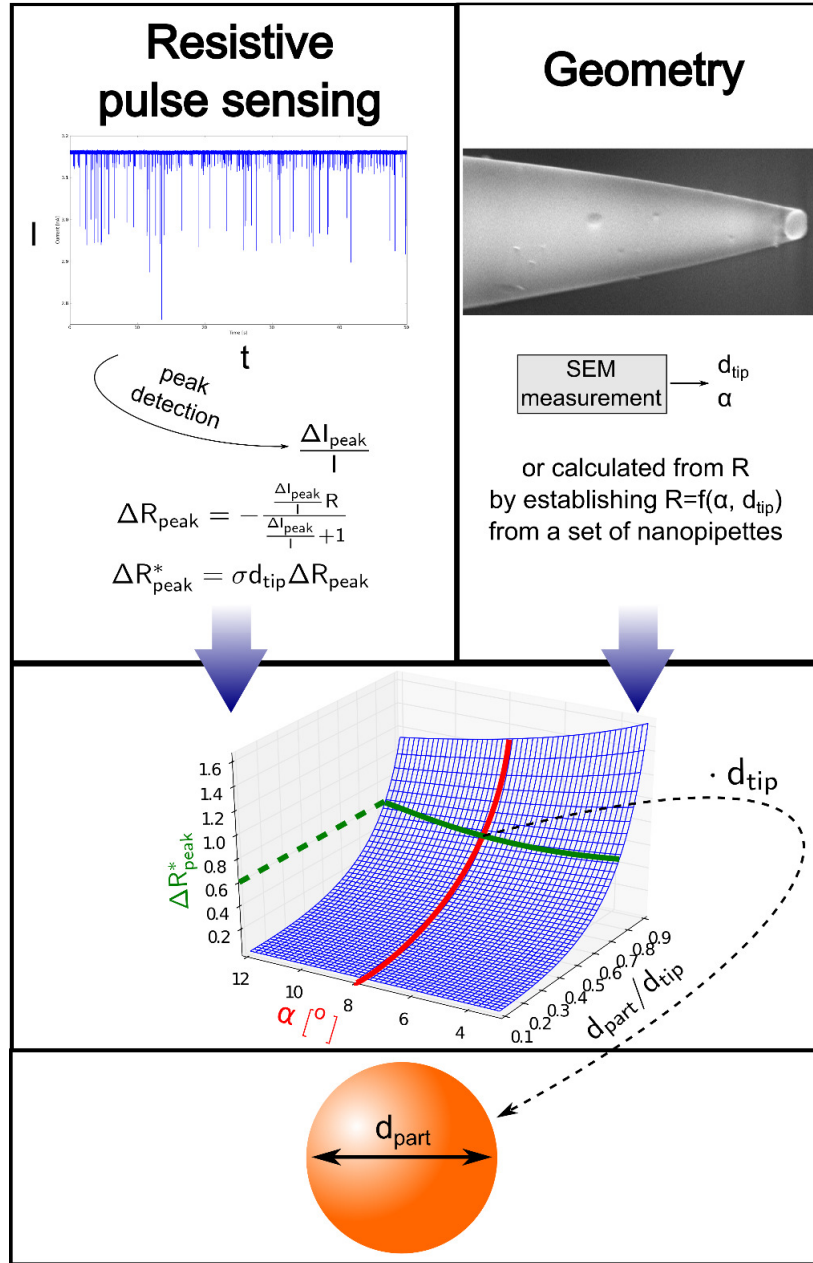**Algorithm for calibration-less sizing of nanoparticles**

The algorithm that is proposed for calibration-less sizing by using nanopipette-based RPS is summarized in Fig. 3. Based on the simple particle translocation model presented above in a solution of given conductivity the amplitude of a resistive pulse is a function of the nanoparticle diameter and the nanopipette geometry, i.e., tip diameter and inner half cone angle.

Therefore, first we have calculated the maximal relative current change of the current pulse/peak caused by the particle translocation for a pertinent range of half cone angles and relative particle sizes. The relative current changes ($\Delta I_{peak}/I$) were then further transformed into resistance changes (ΔR_{peak}) and eventually to normalized resistance changes (ΔR_{peak}^{*}) using the following equations:

$$\Delta R_{peak} = -R\frac{\Delta I_{peak}/I}{\Delta I_{peak}/I + 1} \qquad \text{Eq. 4}$$

$$\Delta R_{peak}^{*} = \sigma d_{tip}\Delta R_{peak} \qquad \text{Eq. 5}$$

11

Using ΔR_{peak}^* instead of ΔR_{peak} is more convenient as it does not require additional calculations for different d_{tip} and σ values along with α and d_{part}/d_{tip}. Plotting ΔR_{peak}^* as a function of the relative particle size and half cone angle of the nanopipette results in a 3D plot as shown in Figure 3 (see also Fig. S5). Thus, if the nanopipette geometry is known the calculation of the nanoparticle diameter should be possible solely based on RPS measurements, without the need for calibration with nanoparticle standards of known diameter. The d_{tip} and α values of the nanopipettes used for RPS measurements were determined by SEM. Accordingly, a large set of nanopipettes with diameters between 50 and 800 nm were prepared, characterized by SEM and the determined geometry was correlated with the electrical resistance measured in 1 M KCl. This allowed at later stage to determine the geometry of the nanopipettes prepared by the single parameter variation method as described in the experimental section solely by measuring their electrical resistance. Thus, to determine the particle size distribution in a suspension the current peaks detected during RPS were identified and the normalized resistance changes corresponding to the maximal relative current change were calculated for each peak. The particle diameter was calculated by implementing into the fitted two-dimensional polynomial equation the geometrical parameters, first α to obtain the relative particle size ($\frac{d_{part}}{d_{tip}}$) and then d_{tip}. Of note, to avoid nanoparticle aggregation the counting measurements were performed in more dilute electrolytes (50 mM KCl or PBS) than the 1 M KCl solution used to measure the nanopipette resistance in rectification-free condition.[55] In this case, the nanopipette resistance measured in 50 mM KCl or PBS were converted to the one that would have been measured in 1 M KCl by using a previously established correlation between the resistances measured in the lower ionic strength electrolytes and 1 M KCl for various nanopipette diameters (Fig. S4).

Figure 3. Overview of the algorithm for the calibration-less determination of the nanoparticle size from nanopipette-based RPS. The experimental input parameters are the geometry of the pore (α and d_{tip} determined by SEM or estimated from the nanopipette resistance), the relative amplitude of the current transients $\left(\frac{\Delta I_{peak}}{I}\right)$ measured during RPS experiments, the nanopipette resistance and the solution conductivity. As shown graphically the intersection of the ΔR^*_{peak} and the half cone

angle in the 3D plot provides the relative particle size and as d_{tip} is known the particle diameter can be ultimately calculated.

RESULTS AND DISCUSSION

Characterization of the nanopipette geometry

The geometry of the fabricated nanopipettes was thoroughly characterized by both SEM and electrical resistance measurements. To use the same nanopipette for SEM and electrochemical measurements is not practical. Therefore, the identical pair of nanopipettes stemming from a single capillary/pull (the deviation of their resistances was typically lower than 1.5% (Table S2)) was used for the two measurements. According to the SEM images the nanopipette cross-sections were slightly elliptic (Fig. 4A) so the tip diameter was calculated as the diameter of a circle of equivalent area.
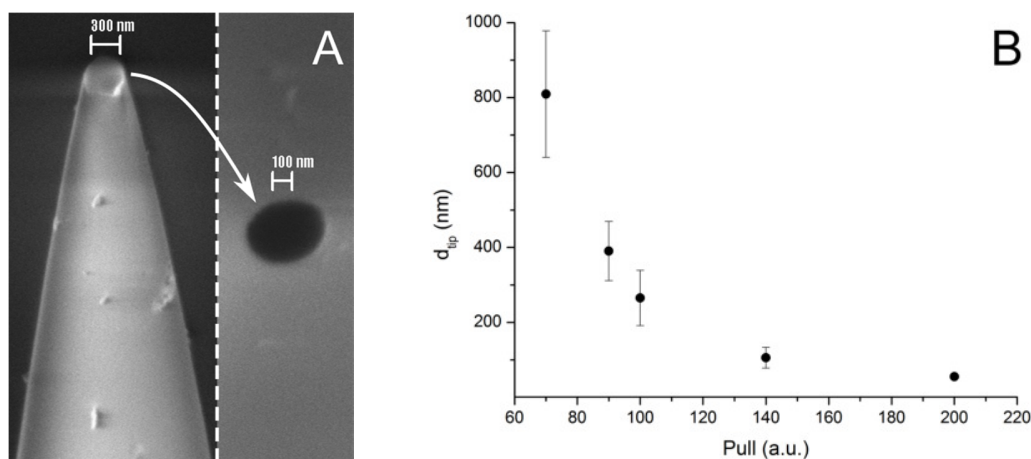

Figure 4. (A) SEM images of a nanopipette with a tip diameter of 300 nm at a stage angle of 45° and 0° to the pipette axis. (B) The SEM determined tip diameter of the nanopipettes as a function of the pull value.

Nanopipettes with tip diameters between ca. 50 and 800 nm were fabricated by setting different pull parameters in the second pulling cycle (Fig. 4B). Adjusting the tip diameter through a single parameter is very convenient, but caused relatively high uncertainties at the larger diameter pipettes. However, the uncertainty decreased for smaller diameter nanopipettes and since these were the focus of the study no further refinement of the pulling parameters was made at this stage. In agreement with others[46] we also found by SEM that the conical shape of the tip is an approximation as the angle of the tip varies along the axis of the nanopipette. Thus, α is in fact the half cone angle right at tip opening. By SEM only the outer angle can be measured, however assuming that the ratio of the inner and outer diameter of the original quartz capillary (γ, in our case $\gamma = \frac{1}{0.7}$) remains constant along the nanopipette,[56] one can calculate the inner half-cone angle as $\alpha = arctan\left(\frac{tan(\alpha_{out})}{\gamma}\right)$. The α values for nanopipettes made by the proposed fabrication method varied in a narrow range of 7-10°, slightly decreasing as the nanopipette diameter decreased (Fig. S6).

Sizing polymeric nanoparticles

To evaluate the sizing capabilities of nanopipettes RPS measurements were performed on suspensions consisting of monodisperse latex nanoparticles as well as on mixtures of closely sized nanoparticle dispersions. Typical transients and processed data for characterizing a monodisperse CML nanoparticle suspension ($\varnothing$=67 nm, 1.5×10^{10} particles/mL) are presented in Fig. 5.
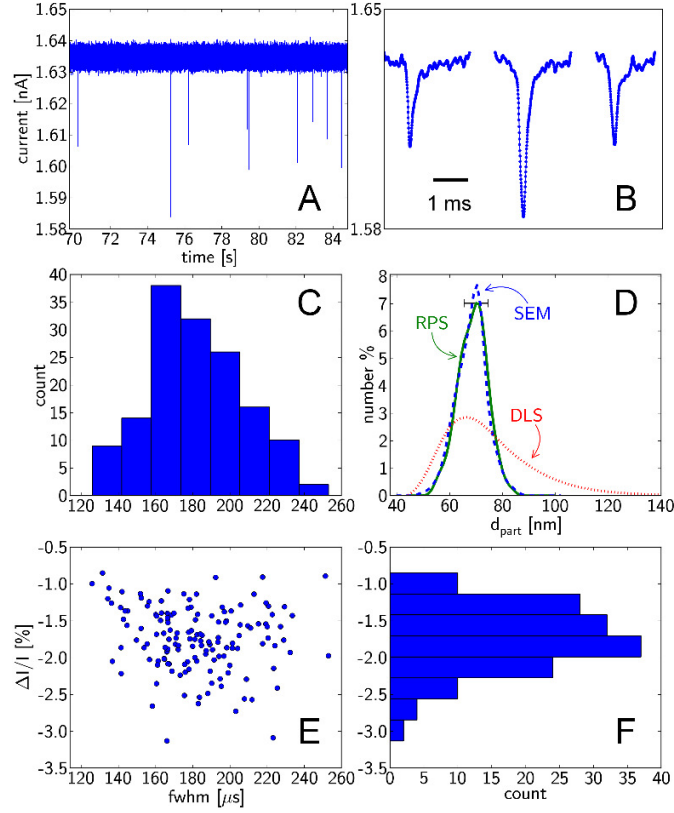
Figure 5. Typical raw current trace (A) with magnified current peaks (B) recorded during the RPS of 67 nm diameter CML particles (1.5×10^{10}/mL). (C,E,F) Event histograms constructed from the detected peaks. (D) Comparison of the size distributions determined by RPS (n=147), SEM (n=312) and DLS. RPS measurements were carried out with a 140 ± 9 nm diameter nanopipette at E_{appl} =100 mV in 50 mM KCl with 0.05 % Triton-X100. The nanoparticle concentration was 1.5×10^{12} /mL for SEM and DLS measurements.

The calibration-less algorithm was used to determine the size distribution shown in Fig. 5B from RPS measurements. We found on excellent agreement between the mean particle diameter determined by nanopipette-based RPS and those stemming from DLS and SEM measurements (Table 1). Moreover, there is an almost perfect overlapping between the RPS and SEM derived

16

size distributions, which is in agreement with results of Fraikin et al.[22] obtained in the same size range, however, with a much more complex fluidic system and detection methodology.

As the next step the nanoparticle sizing was performed in mixtures of monodisperse nanoparticle suspensions. Fig. 6 (Fig. S7 and S8) shows the performance of the RPS method with reassuring results in terms of discriminating closely sized nanoparticle populations.
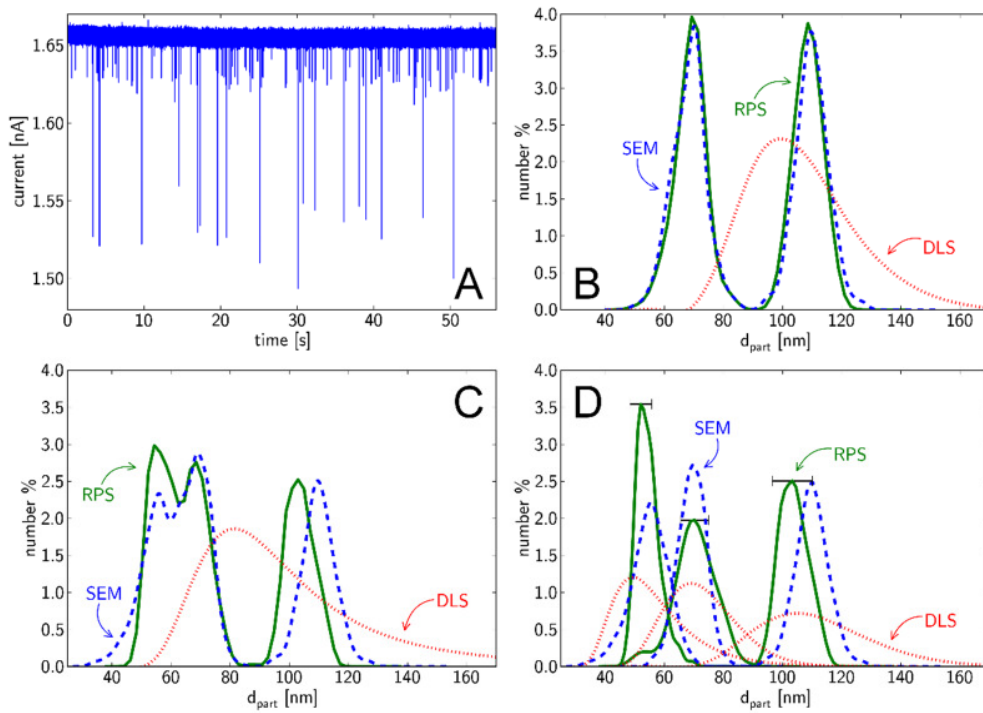
Figure 6. Typical current trace (A) and the corresponding size distributions (B) of a nanoparticle suspension comprising 67 (7.5×10^{10}/mL) and 110 nm (1.5×10^{10}/mL) diameter particles. (C) Size distribution of a suspension comprising a mixture of 45 (4.5×10^{10}/mL), 73 (4.5×10^{10}/mL), and 110 nm (1.5×10^{10}/mL) diameter nanoparticles and (D) overlay of the corresponding individually determined size distributions of the three monodisperse nanoparticle populations. The RPS measurements were carried at E_{appl}=100 mV with different nanopipettes (d_{tip} =142 ± 9 nm) in 50 mM KCl + 0.05 % Triton-X100. For SEM and DLS measurements suspensions with 1.5×10^{12}

particles/mL were used. The particle count ranged between 100 and 600 in RPS measurements and between 250 and 300 in SEM measurements (C, D).

In the studied size range the size resolution of the nanopipette-based measurements were comparable to that of the SEM measurements. However, the DLS measurements well suitable for characterizing monodisperse populations failed to resolve any of the nanoparticle mixtures in the studied size range providing a single peak based distribution (Fig. 6, Figs. S8, S9) consistent with the result of Fraikin et al.[22]. Additionally, the mean particle diameter has much higher uncertainty (Table 1) than either the RPS or SEM in accordance with the observed broad size distributions. Contrary to DLS, the resolving power of SEM and RPS is not limited by the method, but by the inherent dispersity of the nanoparticle suspension. Even for the mixture of closely sized 45 nm and 67 nm "monodisperse" nanoparticles the presence of multiple populations can be clearly distinguished (Fig. 6C). As the nominally 45 nm diameter nanoparticles were found to be by all three techniques close to 55 nm the size discrimination of RPS is even more impressive as the difference between the population means is only ca. 13 nm. This is line with previous results reporting nanopipette based counters able to discriminate between a bare gold nanoparticle and its 24-mer DNA conjugate,[46] which corresponds, if the DNA is in a fully extended conformation, to a difference of ca. 15 nm in diameter. However, this discrimination was based on the difference of the corresponding amplitudes of the current pulses without converting them to size information. Such a size conversion would have enabled to characterize the average thickness of the immobilized layer on the nanoparticle surface as done later by Wang et al. for IgG modified and bare gold nanoparticles, [45] though using a less accurate translocation model that does not consider the out of pore contribution of the nanoparticles to the pulse amplitude. This outlines the

importance of quantitative sizing for an in-depth characterization of nanoparticles in contrast to commonly used unprocessed pulse amplitude data.

Table 1. Comparison of mean particle diameters determined by RPS, SEM and DLS

	Nominal diameter [nm]	Mean diameter ± SD [nm]		
		RPS	SEM	DLS
monodisperse	67	68.7 ± 5.4	68.2 ± 5.7	74.5 ± 15.4
ternary mixture	45	54.6 ± 3.9	54.9 ± 6.4	54.4 ± 12.3
	73	70.2 ± 6.9	69.3 ± 4.6	73.9 ± 10.4
	110	103.8 ± 4.6	109.9 ± 5.5	108.1 ± 18
binary mixture	45	55.6 ± 5.0	54.9 ± 6.4	54.4 ± 12.3
	67	68.7 ± 5.4	68.2 ± 5.7	74.5 ± 15.4

While the mean diameter of the nanoparticles determined by SEM and RPS agreed within the experimental error (Table 1) discrepancies in the shape of the histograms were also observed (Fig 6C). This seems to be caused by the narrow size range of RPS method as the discrepancies in the size distribution are apparent at the edge of the assessable range. In this respect, the SEM determined size distribution of the 45 nm nominal diameter particles exhibits a "tail" extending below 40 nm range which is absent in the size distribution derived from nanopipette-based counting. This is because the current pulses made by those particles are below the current noise threshold of the 142 nm diameter nanopipette used to cover the size range of the ternary mixture.

Determination of the nanoparticle concentrations

The translocation event frequency f_{event} scales linearly[47] with the concentration of the nanoparticles as long as the concentration is low enough to avoid particle-particle interactions and this basic dependency was confirmed in this study (Fig. S11). Consequently, the nanoparticle concentration can be determined based on previous calibration with relevant nanoparticle

concentration standards. However, the slope of the calibration curves can differ from particle to particle owing to their different size and/or surface charge density that determines their electrical mobility. Therefore, a calibration with nanoparticle standards should be performed for each type of nanoparticle, which is very difficult and impractical. Alternatively, if the volume of liquid drawn under pressure through the nanopipettes is known, relating it to the event frequency would allow for a calibration-less concentration determination in a similar way as in commercial Coulter counters using micrometer diameter apertures. However, the flow rate established through nanopores is generally too small (pL/min or less) to be directly and accurately measured. This limitation can be overcome by calculating the hydrodynamic resistance (R_H) of the nanopipette, which, if the applied pressure (P) is known, can be used to calculate the volume flow (Q) through the pore.

$$Q = \frac{P}{R_H} \qquad \text{Eq. 6}$$

Recently the expression for the hydrodynamic resistance of conical geometry pores was derived based on the Hagen-Poiseuille equation[17, 57] to allow the calibration-less assessment of nanoparticle concentrations with elastomeric nanopores.[17]

In case of a nanopipette the hydrodynamic resistance of the sensing zone dominates the overall hydrodynamic resistance of the system (based on our calculation 95% of the hydrodynamic resistance of the nanopipette is given by the conical tip segment having a height of 6×d$_{tip}$ (Fig. S12).Therefore, the nanopipette can be treated as having an ideal conical geometry:[17, 57, 58]

$$R_{H,l}^{pipette} = \frac{8\mu}{\pi} \int_{x=0}^{l} \frac{1}{r(x)^4} \, dx = \frac{128 l \mu \left(3 d_{tip}^2 + 6 \tan(\alpha) l d_{tip} + 4 \tan(\alpha)^2 l^2 \right)}{3 \pi d_{tip}^3 \left(d_{tip} + 2 \tan(\alpha) l \right)^3} \qquad \text{Eq. 7}$$

where μ is the dynamic viscosity of the solution and l is the length of the cone.

The expression is further simplified by considering that the pipette tip is at least 3 orders of magnitude longer than the tip diameter:

$$\lim_{l \to \infty} R_{H,l}^{pipette} = R_H^{pipette} = \frac{64\mu}{3\pi d_{tip}^3 tan(\alpha)} \qquad \text{Eq. 8}$$

The streamlines of the solution outside the pipette are converging to the nanopipette orifice and create a hydrodynamic access resistance, which was approximated by the half of the hydrodynamic resistance measured across an aperture with d_{tip} diameter ($R_H^{access} = \frac{12\mu}{d_{tip}^3}$).[59] Thus the overall hydrodynamic resistance is given by $R_H = R_H^{pipette} + R_H^{access}$. The particle concentration can be evaluated by calculating the hydrodynamic resistance and measuring the event frequency:

$$c_{part} = \frac{f_{event}}{P} R_H \qquad \text{Eq. 9}$$

However, Eq. 9 is valid only if the hydrodynamic is the sole transport mechanism, i.e., if the f_{event}–pressure calibration line goes through the origin, which is seldom the case. This limitation can be overcome by substituting the $\frac{f_{event}}{P}$ ratio by $\frac{\Delta f_{event}}{\Delta P}$, where Δf_{event} is the event frequency change corresponding to a given applied pressure change ΔP:

$$c_{part} = \frac{\Delta f_{event}}{\Delta P} R_H \qquad \text{Eq. 10}$$

This allows to calculate the volume flow through the nanopipette and calculate the particle concentration from the slope of a linear event frequency – pressure curve (Fig. 7A). Of note, there might be deviation from linearity at high and low applied pressures, therefore, a multipoint calibration is preferred against a two-point[17] approach. The non-zero intercept is due to the combined effect of the inward directed electrophoretic force acting on the negative charged particles and the capillary pressure (200-300 Pa) induced inward flow of the solution.
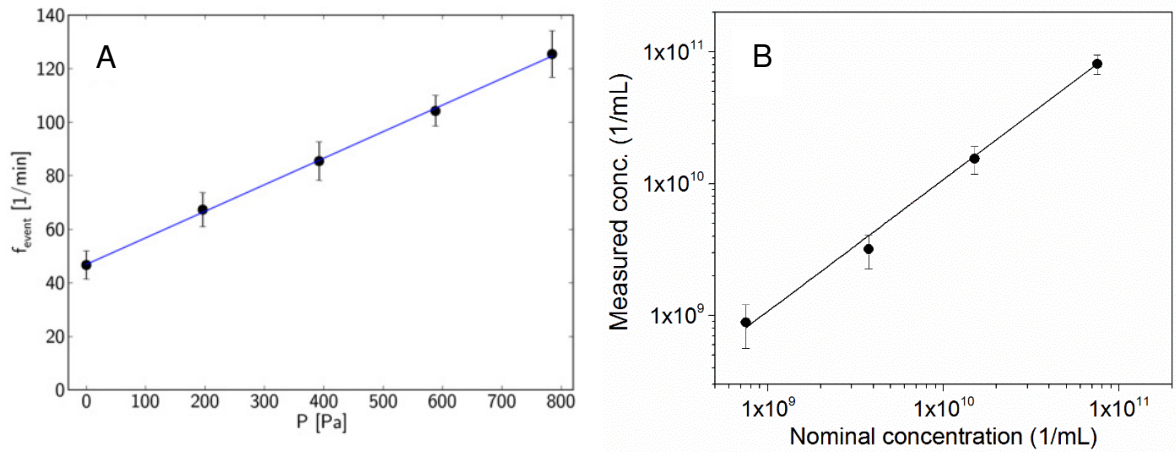
Figure 7. (A) Event frequency of 67 nm diameter CML nanoparticle translocations as a function of the applied pressure at a nominal particle concentration of 7.5×10^{10}/mL ($\boldsymbol{d_{tip}} = 145 \pm 10$ nm). (B) Correlation between concentrations determined by RPS and nominal values for 73 nm diameter CML nanoparticle suspensions in PBS ($E_{app} = 100$ mV, $\boldsymbol{d_{tip}} = 162 \pm 10$ nm).

Fig. 7B illustrates the correlation between concentrations determined with the calibration-less RPS method and nominal values provided by the manufacturer for the 73 nm diameter CML nanoparticles. The error bars were determined by error propagation calculation considering the uncertainties of all parameters involved. The measured concentrations are ca. 8 % larger than the nominal value and a similar overestimation was observed for 110 nm diameter particles. Since there are no certified concentration standards available for such nanoparticles it is difficult to ascertain the exact origin of this bias. The deviation could be stemming from the fact that the manufacturer provides only the w/v% of the nanoparticle suspension, i.e., the mass of dry matter in the solution. This is converted to number concentration using the density and the nominal diameter of the nanoparticle. Thus the accuracy of the nanoparticle diameter is essential for concentration calculation and the uncertainty of the nanoparticle diameters seem to account for the

observed discrepancy. The accuracy of the results are in agreement with those obtained by Roberts et al. with elastomeric nanopores (2 to 17%),[17] however, for much larger polymeric particles and bacteria than used in this study, i.e., with diameters between ca. 200 nm and 1 µm.

Characterization of poliovirus samples

Counting viruses is more challenging than counting well stabilized synthetic nanoparticles, as viruses are known to be susceptible to aggregation and, additionally, adsorption onto nanopipettes might also occur. Studies suggest that poliovirus suspensions behave like classical colloids[60] but in case of aggregation significant deviations exist. Though counter-intuitive, because repulsive electrostatic forces should hinder aggregation, poliovirus aggregation is more significant at low ionic strength.[61, 62] Aggregation occurs also at a pH below 6-7[63, 64] although the isoelectric point of the virus is around 8,[64, 65] which indicates that the virus is effectively positively charged in this pH-range. Since, Young and Sharp[62] found PBS to be remarkably efficient in preventing and/or reversing poliovirus aggregation, we used PBS to suspend the poliovirus samples in our RPS experiments, adding 0.05% Tween-20 to aid the wetting of the nanopipette.
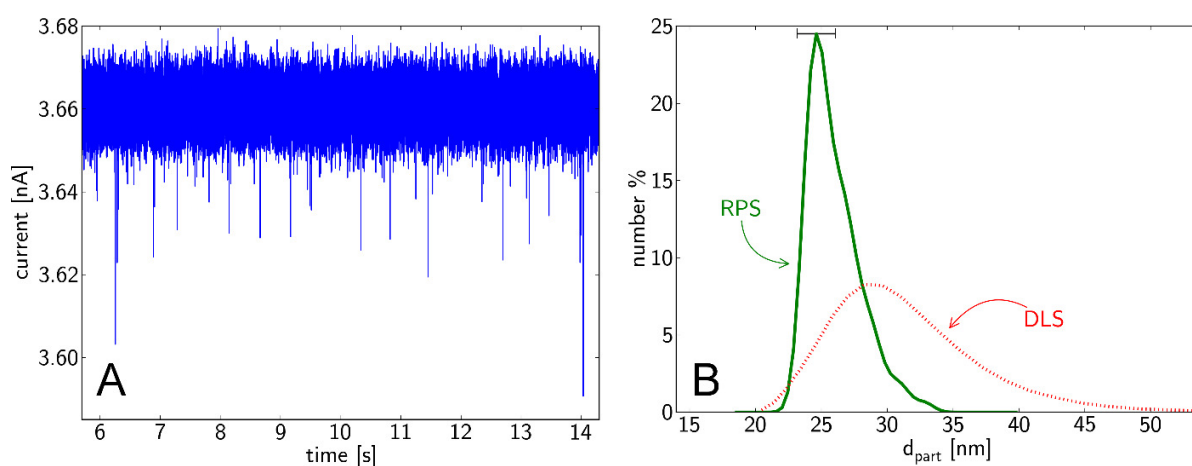
Figure 8. (A) Typical current signal (after baseline drift correction) with peaks originating from the translocation of inactivated poliovirus particles through a 53 ± 3 nm diameter nanopipette. (B) Size distribution of inactivated poliovirus particles determined by RPS (N=286) and DLS measurements. Measurements were performed in PBS at E_{appl} = 300 mV. The virus stock solution was diluted 15-fold for RPS and 3-fold for DLS measurements.

The RPS measurements provided a mean diameter of 26 ± 1.9 nm for the poliovirus particles while the DLS measurements 32.6 ± 4.5 nm both within the range of 24-30 nm reported previously.[33-35] Comparing the size distributions obtained by RPS and DLS (Fig. 8) suggests that the narrower size range of the nanopipette-based counting can constitute an advantage when it is used as a size-selective sensor, i.e., tuned to detect particles of interest within a given size range. The broad distribution provided by DLS is most likely biased towards larger size by aggregates, while the ca. 50 nm nanopipette is sensing dominantly the non-aggregated virus particles with results characteristic of the inherent monodispersity of the poliovirus. Since the concentration of the poliovirus samples were unknown, to validate the concentrations determined by RPS we adopted a method suggested by Vysotskii et al.[66] for the determination of nanoparticle concentrations based on static light scattering measurements. As the virus diameter is much smaller than the wavelength of the illuminating laser used in the DLS instrument (633 nm) it can be can be treated as a Rayleigh-scatterer. Consequently, the virus concentration can be estimated by relating it to another Rayleigh-scatterer used as standard, e.g., a CML nanoparticle with known diameter and concentration as follows:

$$\frac{c_{virus}}{c_{standard}} = \frac{I_{virus}}{I_{standard}} \left(\frac{d_{standard}}{d_{virus}}\right)^6 \left[\frac{\left(\frac{n_{standard}}{n_{solution}}\right)^2 - 1}{\left(\frac{n_{standard}}{n_{solution}}\right)^2 + 2} \frac{\left(\frac{n_{virus}}{n_{solution}}\right)^2 + 2}{\left(\frac{n_{virus}}{n_{solution}}\right)^2 - 1}\right]^2 \qquad \text{Eq. 11}$$

where c_{virus} and $c_{standard}$ are the virus and standard concentration, d_{virus} and $d_{standard}$ are the virus and the standard (CML nanoparticle) nanoparticle diameter, I_{virus} and $I_{standard}$ are the scattered light intensity stemming from the virus and the standard. The refractive indices of the solution, as well as of the standard and virus particles used in Eq. 11 were $n_{solution}$=1.332, $n_{standard}$=1.590 (CML latex), n_{virus}=1.450, respectively. By this method the dominant source of error is the uncertainty of the diameters of the standard and virus particles because their ratio in Eq. 11 is at the 6th power. The concentration of the virus stock solution was determined by the static light scattering method for both 25 and 45 nm CML nanoparticles used as standards. The resulting virus concentrations were in fairly good agreement despite of the sensitivity of the method to the particle diameter (Table 2). The virus concentrations determined by calibration-less RPS measurements and static light scattering also agreed within the experimental error, but the uncertainty of the virus concentration determined by RPS was significantly smaller.

Table 2. Concentration of poliovirus-S1 stock solution determined by static light scattering and RPS measurements. Both determinations were made in PBS solution (pH 7.4) with 0.05% Tween-20.

Static light scattering			
diameter of the standard CML nanoparticle [nm]	concentration [1/mL]		relative error [%]
25	1.17×10^{13}		64.0
45	8.14×10^{12}		53.9
Resistive pulse sensing			
d_{tip}[nm]	α [deg]	R_H [Pa×min/pL]	concentration [1/mL]	relative error [%]
53.1 ± 2.81	6.3 ± 0.74	7417 ± 1617	6.75×10^{12}	23.1

53.4 ± 2.85	6.4 ± 0.76	7133 ± 1562	6.075×10^{12}	23.0

CONCLUSIONS

The calibration-less sizing approach by using nanopipette-based RPS proved to provide for all nanoparticles in this study mean diameters that agreed well with values stemming from SEM and DLS measurements. In most cases the difference between the diameters determined by RPS and SEM was less than 1.5 %. Similar to SEM, the nanopipette-based RPS determinations can readily resolve mixtures of nanoparticles with close size distributions (tested down to 13 nm), where DLS fails and provides a single peak distribution. The concentration of nanoparticles determined by the calibration-free approach were ca. 8 % higher than the nominal values provided by the manufacturer based on gravimetric measurement. This is fairly negligible bias at such low concentrations well within the experimental error of the two techniques. Both the calibration-free sizing and quantitation proved to be suitable for characterizing poliovirus particles, the smallest spherical shaped virus ever investigated by RPS. A static light scattering method was additionally worked out to validate the poliovirus concentration determined by the nanopipette-based RPS measurements, and the values obtained by the two methods agreed within the experimental error. The results suggest that the simple particle translocation model coupled with nanopipette-based RPS is appropriate for the calibration-free sizing and quantitation of insulating nanoparticles in the lower nanometer range. Considering, also the ease and cost effectiveness of nanopipette fabrication further studies along this line are in perspective.

Supporting Information. "This material is available free of charge via the Internet at http://pubs.acs.org."

ACKNOWLEDGMENT

REFERENCES

1. J. J. Kirkland, *J. Chromatogr.* 1979, *185*. 273.
2. M. Baalousha, B. Stolpe, J. R. Lead, *J. Chromatogr. A* 2011, *1218*. 4078.
3. X. Xu, K. K. Caswell, E. Tucker, S. Kabisatpathy, K. L. Brodhacker, W. A. Scrivens, *J. Chromatogr. A* 2007, *1167*. 35.
4. T. Svedberg, H. Rinde, *J. Am. Chem. Soc.* 1924, *46*. 2677.
5. V. Filipe, A. Hawe, W. Jiskoot, *Pharm. Res.* 2010, *27*. 796.
6. M. Wright, in *Nanoparticles in Biology and Medicine*, ed. M. Soloviev. Humana Press, 2012, vol. 906, pp 511.
7. H. Bayley, C. R. Martin, *Chem. Rev.* 2000, *100*. 2575.
8. X. Y. Xiao, A. J. Bard, *J. Am. Chem. Soc.* 2007, *129*. 9610.
9. Y. G. Zhou, N. V. Rees, R. G. Compton, *Angew. Chem. Int. Ed* 2011, *50*. 4219.
10. O. A. Saleh, L. L. Sohn, *Rev. Sci. Instrum* 2001, *72*. 4449.
11. Q. Zhenpeng, Z. Jiang, W. Guo-Xiang, *Meas. Sci. Technol.* 2011, *22*. 045804.
12. H. Liu, S. Qian, H. H. Bau, *Biophys. J.* 2007, *92*. 1164.
13. S. W. Joo, S. Qian, *J. Colloid Interface Sci.* 2011, *356*. 331.
14. D. A. Holden, G. Hendrickson, L. A. Lyon, H. S. White, *J. Phys. Chem. C* 2011, *115*. 2999.
15. R. Vogel, W. Anderson, J. Eldridge, B. Glossop, G. Willmott, *Anal. Chem.* 2012, *84*. 3125.
16. T. Ito, L. Sun, R. M. Crooks, *Anal. Chem.* 2003, *75*. 2399.
17. G. S. Roberts, S. Yu, Q. Zeng, L. C. L. Chan, W. Anderson, A. H. Colby, et al., *Biosensors and Bioelectronics* 2012, *31*. 17.
18. K. R. Balakrishnan, G. Anwar, M. R. Chapman, T. Nguyen, A. Kesavaraju, L. L. Sohn, *Lab Chip* 2013, *13*. 1302.
19. R. W. Deblois, C. P. Bean, *Rev. Sci. Instrum* 1970, *41*. 909.
20. J. D. Uram, K. Ke, A. J. Hunt, M. Mayer, *Small* 2006, *2*. 967.
21. Z. D. Harms, K. B. Mogensen, P. S. Nunes, K. Zhou, B. W. Hildenbrand, I. Mitra, et al., *Anal. Chem.* 2011, *83*. 9573.
22. J.-L. Fraikin, T. Teesalu, C. M. McKenney, E. Ruoslahti, A. N. Cleland, *Nat Nano* 2011, *6*. 308.
23. R. Vogel, G. Willmott, D. Kozak, G. S. Roberts, W. Anderson, L. Groenewegen, et al., *Anal. Chem.* 2011, *83*. 3499.
24. J. J. Kasianowicz, E. Brandin, D. Branton, D. W. Deamer, *Proc. Natl. Acad. Sci.* 1996, *93*. 13770.

25. C. C. Harrell, Y. Choi, L. P. Horne, L. A. Baker, Z. S. Siwy, C. R. Martin, *Langmuir* 2006, *22*. 10837.

26. L. T. Sexton, H. Mukaibo, P. Katira, H. Hess, S. A. Sherrill, L. P. Horne, et al., *J. Am. Chem. Soc.* 2010, *132*. 6755.

27. E. A. Heins, Z. S. Siwy, L. A. Baker, C. R. Martin, *Nano Lett.* 2005, *5*. 1824.

28. H. Bayley, P. S. Cremer, *Nature* 2001, *413*. 226.

29. S. Howorka, S. Cheley, H. Bayley, *Nat Biotech* 2001, *19*. 636.

30. Z. Siwy, L. Trofin, P. Kohli, L. A. Baker, C. Trautmann, C. R. Martin, *J. Am. Chem. Soc.* 2005, *127*. 5000.

31. R. R. Henriquez, T. Ito, L. Sun, R. M. Crooks, *Analyst* 2004, *129*. 478.

32. K. Zhou, L. Li, Z. Tan, A. Zlotnick, S. C. Jacobson, *J. Am. Chem. Soc.* 2011, *133*. 1618.

33. A. Polson, G. Selzer, *Biochim. Biophys. Acta* 1957, *24*. 597.

34. H. O. Agrawal, *Archiv. f. Virusforschung* 1966, *19*. 365.

35. R. Floyd, *Appl. Environ. Microbiol.* 1979, *38*. 980.

36. R. E. Gyurcsányi, *TrAC, Trends Anal. Chem.* 2008, *27*. 627.

37. S. Majd, E. C. Yusko, Y. N. Billeh, M. X. Macrae, J. Yang, M. Mayer, *Curr. Opin. Biotechnol.* 2010, *21*. 439.

38. H. Bayley, L. Jayasinghe, *Mol. Membr. Biol.* 2004, *21*. 209.

39. M. Davenport, K. Healy, M. Pevarnik, N. Teslich, S. Cabrini, A. P. Morrison, et al., *ACS Nano* 2012, *6*. 8366.

40. R. W. Deblois, C. P. Bean, R. K. A. Wesley, *J. Colloid Interface Sci.* 1977, *61*. 323.

41. S. Wu, S. R. Park, X. S. Ling, *Nano Lett.* 2006, *6*. 2571.

42. O. A. Saleh, L. L. Sohn, *Nano Lett.* 2002, *3*. 37.

43. B. Zhang, J. Galusha, P. G. Shiozawa, G. L. Wang, A. J. Bergren, R. M. Jones, et al., *Anal. Chem.* 2007, *79*. 4778.

44. W.-J. Lan, D. A. Holden, B. Zhang, H. S. White, *Anal. Chem.* 2011, *83*. 3840.

45. Y. Wang, K. Kececi, M. V. Mirkin, V. Mani, N. Sardesai, J. F. Rusling, *Chem. Sci.* 2013, *4*. 655.

46. M. Karhanek, J. T. Kemp, N. Pourmand, R. W. Davis, C. D. Webb, *Nano Lett.* 2005, *5*. 403.

47. L. Sun, R. M. Crooks, *J. Am. Chem. Soc.* 2000, *122*. 12340.

48. T. Ito, L. Sun, M. A. Bevan, R. M. Crooks, *Langmuir* 2004, *20*. 6940.

49. C. A. Morris, A. K. Friedman, L. A. Baker, *Analyst* 2010, *135*. 2190.

50. D. Kozak, W. Anderson, R. Vogel, S. Chen, F. Antaw, M. Trau, *ACS Nano* 2012, *6*. 6990.

51. D. Kozak, W. Anderson, M. Grevett, M. Trau, *J. Phys. Chem. C* 2012, *116*. 8554.

52. G. R. Willmott, B. E. T. Parry, *J. Appl. Phys.* 2011, *109*. 094307.

53. Z. Siwy, A. Fuliński, *Am. J. Phys* 2004, *72*. 567.

54. J. E. Hall, *J. Gen. Physiol.* 1975, *66*. 531.

55. C. Wei, A. J. Bard, S. W. Feldberg, *Anal. Chem.* 1997, *69*. 4627.

56. D. C. Dung, H. L. Nghia, V. P. Veiko, A. O. Golubok, E. B. Yakovlev, in *The Third International Conference on the Development of Biomedical Engineering in Vietnam*, ed. V. V. Toi, T. Q. D. Khoa. Springer Berlin Heidelberg, 2010, pp 127.

57. W.-J. Lan, D. A. Holden, J. Liu, H. S. White, *J. Phys. Chem. C* 2011, *115*. 18445.

58. W. P. Walawender, P. Prasassarakich, *Microvasc. Res.* 1976, *12*. 1.

59. T. B. Sisan, S. Lichter, *Microfluid. Nanofluid.* 2011, *11*. 787.

60. R. Floyd, D. G. Sharp, *Appl. Environ. Microbiol.* 1978, *35*. 1079.

61. R. Floyd, D. G. Sharp, *Appl. Environ. Microbiol.* 1977, *33*. 159.

62. D. C. Young, D. G. Sharp, *Appl. Environ. Microbiol.* 1977, *33*. 168.

63. R. Floyd, D. G. Sharp, *Appl. Environ. Microbiol.* 1978, *35*. 1084.

64. R. Floyd, D. G. Sharp, *Appl. Environ. Microbiol.* 1979, *38*. 395.

65. A. Hamann, C. Reichel, K. J. Wiegers, R. Drzeniek, *J. Gen. Virol.* 1978, *38*. 567.

66. V. V. Vysotskii, O. Y. Uryupina, A. V. Gusel'nikova, V. I. Roldugin, *Colloid J.* 2009, *71*. 739.